Journal of Molecular Liquids 325 (2021) 115208

Contents lists available at ScienceDirect

Journal of Molecular Liquids

journal homepage: www.elsevier.com/locate/molliq

Raman and theoretical studies on structural evolution of Li_2BeF_4 and binary LiF-BeF_2 melts

Yangjuan Li [a,b], Xiyan Liu [a,b], Baozhu Wang [a], Chenyang Wang [a,b,*]

[a] Department of Radiochemistry, Shanghai Institute of Applied Physics, Chinese Academy of Sciences, Shanghai 201800, China
[b] School of Nuclear Science and Technology, University of Chinese Academy of Sciences, Beijing 100049, China

ARTICLE INFO

Article history:
Received 30 November 2020
Received in revised form 19 December 2020
Accepted 23 December 2020
Available online 26 December 2020

Keywords:
Raman spectroscopy
Density functional theory
Li_2BeF_4
LiF-BeF_2 melts

ABSTRACT

The structural evolution of Li_2BeF_4 from crystalline to molten states has been investigated by Raman spectroscopic technique with the assist of density functional theory (DFT). The experimental results of temperature-dependent Raman spectra of Li_2BeF_4 showed that no solid-state phase transformation was taken place during heating process from 298 to 723 K. In the molten state, the structure of BeF_4^{2-} anion was affected by Li^+ cation and environment. For the binary LiF-BeF_2 melts with varying LiF/BeF_2 ratio, the stretching bands of beryllium-fluorine bonds in molten Raman spectra were deconvolved identified by Gaussian function. When the concentration of BeF_2 exceeding 33 mol%, the dimer $Be_2F_7^{3-}$ was formed and dominated the spectrum. It was characterized to have a linear Be–F–Be geometry with two BeF_4 moieties bridged by a single fluorine atom. A second anion $Be_3F_{10}^{4-}$ processing a triple chain structure formed when the content of BeF_2 increasing to 50 mol%. When the concentration of BeF_2 went beyond 60 mol%, the Raman intensity and band width gradually decreased. While the intensity and band width of Raman spectra gradually decreased with the concentration of BeF_2 exceeding to 60 mol%, which suggests that the band should be assigned to a hexatomic $Be_6F_{18}^{6-}$ ring which was similar to the situation in the pure BeF_2 network structure.

1. Introduction

The molten salt reactor (MSR) is one of generation IV nuclear reactor which provide a series of advantages on safety requirements and nuclear source extension [1,2]. Li_2BeF_4 (FLiBe) is selected as a coolant or a fuel salt for MSR due to the effective heat transfer fluid, low absorption and high radiation flux conditions [3,4]. As the best medium for reprocessing thorium based fuel, much more attention has been paid on the properties of the system which was a high-temperature solvent for transition metal ions. Furthermore, the binary LiF-BeF_2 system also needs to be investigated on the properties change with composition [5]. Due to the toxicity of beryllium and corrosion of melt, there have been no clear conclusions of structures for Li_2BeF_4 from the crystalline to molten state and binary LiF-BeF_2 melts.

Extensive studies have been carried out on the crystal structure of Li_2BeF_4 [6–8]. BeF_4^{2-} was formed and combined with two Li^+ to make neutral molecule of Li_2BeF_4 at room temperature [8]. According to Raman spectroscopy, the BeF_4^{2-} and $Be_2F_7^{3-}$ were all present in molten AF-BeF_2 (A = Li, Na) mixtures [9,10]. Besides the experimental method, theoretical calculations were also performed. First-principles basis was used to describe interaction potential for BeF_2 and its mixtures with LiF [11,12]. The infrared spectra of BeF_4^{2-}, $Be_2F_7^{3-}$ and $Be_3F_{10}^{4-}$ in the gas phase were clearly assigned by comparison to the normal mode analysis results [13,14].

Raman spectroscopy is confirmed to be an effective tool to study the local structure of melts [15,16]. In the present paper, the structural evolution of Li_2BeF_4 from the crystalline to molten state has been studied by combining Raman and theoretical calculation. A suitable model and method is proposed for describing molten Li_2BeF_4, and the spectral differences between the crystalline and the molten state were discussed. Furthermore, the binary LiF-BeF_2 melts were also studied on the local structures and mechanism with the variation concentration of BeF_2.

2. Experimental and theoretical methods

The alkali fluoride LiF was purchased from Sigma-Aldrich with 99.99% purity. It was further purified by cooling slowly from the melt to crystal in a glassy carbon crucible. The BeF_2 and Li_2BeF_4 were supplied by Shanghai institute of applied physics [17], and dried under vacuum for 8 h at 473 K before use. To prepare the binary molten LiF-BeF_2 samples, BeF_2 mixed with LiF at a specific molar ratio in platinum crucibles and heated to the molten state according to the phase diagram (Fig. S1 in supplementary material) [18]. All the operations were handled in an argon glove box with oxygen and water content below 1 ppm. In

* Corresponding author at: Department of Radiochemistry, Shanghai Institute of Applied Physics, Chinese Academy of Sciences, Shanghai 201800, China.
E-mail address: wangchenyang@sinap.ac.cn (C. Wang).

https://doi.org/10.1016/j.molliq.2020.115208
0167-7322/

addition, the oxygen contents of these chemicals are less than 300 ppm determined by LECO O836 oxygen analyzer.

For recording the Raman spectra, the Horiba Jobin-Yvon LabRAM HR800 Raman spectrometer was used and equipped with a charge coupled device (CCD) detector. Both 325 and 532 nm laser were used as the excitation sources to investigate the effect of the laser wavelength on the Raman spectrum. The 10× objective lens was adopted to focuse on the samples. The spectra were acquired by an accumulated mode of 10 × 10, which was 10 times with 10 s for each time. In order to obtain the spectral polarization properties, the vertical-vertical (VV) and horizonal-vertical (HV) polarization configurations were used.

Because the Cambridge Serial Total Energy Package (CASTEP) based on density functional theory (DFT) is a powerful tool for studying three-dimensional periodic systems [19,20], exchange and correlation energies were approximated using the Perdew-Burke-Ernzerhof (PBE) functional of generalized gradient approximation (GGA) [21]. The plane-wave energy cutoff and the convergence criterion of the self-consistent field (SCF) were 850 eV and 1.0 e−6 eV/atom, respectively. The Brillouin zone integrations were done over a 2 × 2 × 2 Monkhorst-Pack grid. As to the simulation of finite scale system, Gaussian 09 package is efficient for the melts [22]. *Ab initio* calculation was all employed for geometry optimization and vibrational frequency calculations with Hartree-Fock (HF) /6–311+G(d) basis set [23].

3. Results and discussion

3.1. Room temperature Raman spectrum of Li_2BeF_4 crystal

Li_2BeF_4 is isomorphous compounds with the same unit cell dimensions. The crystal structure was redetermined and belonged to the trigonal crystal system with the R-3H space group [24,25]. The unit cell dimensions are: a = 13.29(1), b = 13.29(1) and c = 8.91(3) Å. The schematic unit cell of Li_2BeF_4 viewed along the XOZ plane was present in Fig. 1. The central Be atom was surrounded by four F atoms and existed at the form of BeF_4^{2-} anion. The calculated Raman spectrum of the Li_2BeF_4 crystal at the GGA/PBE level of theory was shown in Fig. 2 in comparison with the experimental spectrum at room temperature. According to the standard group theory analysis, the vibrational modes were distributed among the following irreducible representations: $21A_u+21E_u+21E_g+21A_g$, where only E_g and A_g modes were Raman-active based on the selection rules. The calculated and experimental results agreed with each other extremely well not only in the peak positions but also in the relative intensities. The calculated Raman shifts of the Li_2BeF_4 crystal were in good agreement with the experimental results (the error was within 15 cm^{-1}). However, two

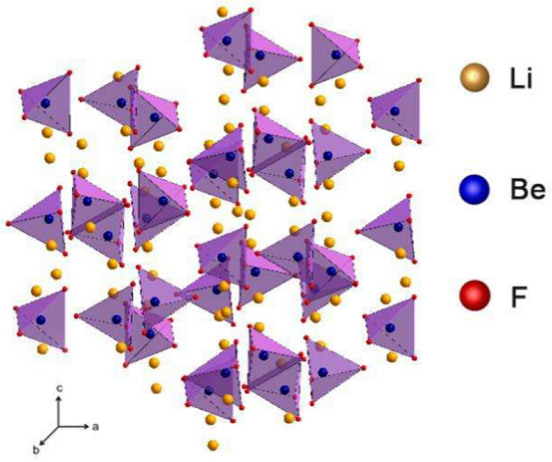

Fig. 1. The crystal packing structure of Li_2BeF_4.

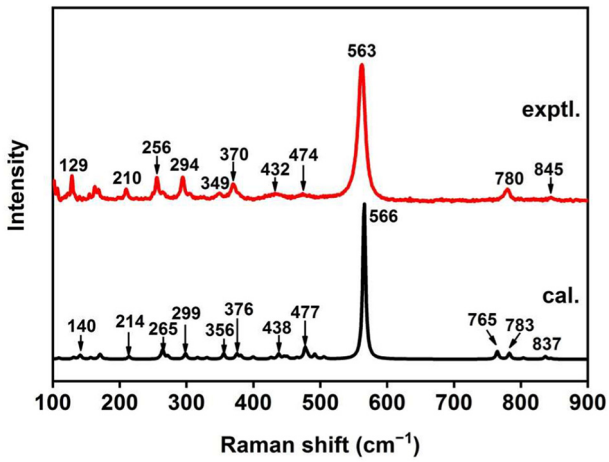

Fig. 2. Calculated and experimental Raman spectra of the Li_2BeF_4 crystal.

calculated bands were obtained at 765 and 783 cm^{-1}, only one band was observed at 780 cm^{-1}. This was caused by the energy of different excitation wavelength, and the other band was not obvious in the spectrum by the 532 nm exciting laser (Fig. S2 in supplementary material).

3.2. Temperature-dependent Raman spectra of Li_2BeF_4

Temperature-dependent Raman spectra of Li_2BeF_4 from room temperature to 823 K were shown in Fig. 3. Further increasing the temperature above 873 K caused partial sample evaporating onto the quartz window of the hotstage. Slight red shifts within 3 cm^{-1} were observed in the Raman spectra obtained below 773 K in Fig. 3. It suggested that there was no solid-state phase transformation reaction. When the temperature increased above 773 K, the observed Raman band of the symmetrical Be–F stretching vibration shifted to 551 cm^{-1}, while other bands were unconspicuous and only two weak bands were observed at 240 and 377 cm^{-1} (Fig. S3 in supplementary material). Polarization measurements of molten Li_2BeF_4 revealed that the band at 551 cm^{-1} disappeared while the intensities of the 240 and 377 cm^{-1} bands were reduced by 0.25 with HV configuration. Similar situation was observed on the variation from crystalline compounds to melts [26,27].

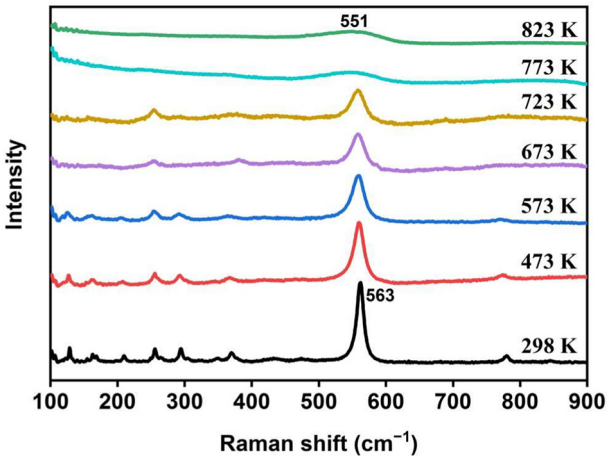

Fig. 3. Temperature-dependent Raman spectra of the Li_2BeF_4 crystal from room temperature to 823 K.

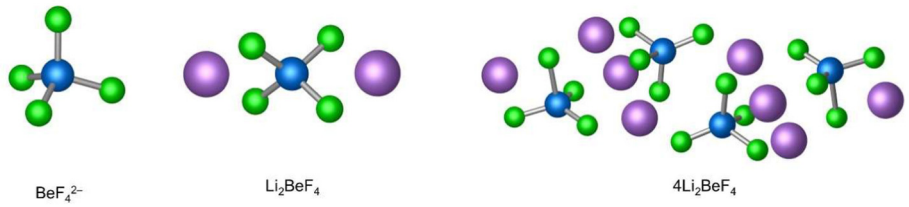

Fig. 4. Optimized geometries of BeF_4^{2-}, Li_2BeF_4 and $4Li_2BeF_4$ at HF/6–311+G(d) level of theory (Be: blue, F:green, Li: purple).

3.3. Calculated Raman spectra of molten Li_2BeF_4

In order to confirm the assignment of the bands observed in molten Li_2BeF_4, *ab initio* calculation was carried out on BeF_4^{2-} anion. Simultaneously, the lithium ion and polymolecular structure were also taken into consideration as shown in Fig. 4. As to the isolated BeF_4^{2-} anion, the theoretical bands are located at 230 cm^{-1} [$\nu_2(E)$], 346 cm^{-1} [$\nu_4(F_2)$] and 489 cm^{-1} [$\nu_1(A_1)$] (Fig. 5). The discrepancy between theoretical and experimental band of Be–F symmetric stretch vibration is about 62 cm^{-1}. In addition, the relative intensity of the calculated bands also indicates that the properties of BeF_4^{2-} were strongly affected by the environment. The bond dissociation energies of Be–F and Li–F are 573 and 577 ± 21 kJ/mol, respectively [28]. Due to the similar energy, the Li^+ ion should be taken into account in geometry optimization. However, the mixtures should be still dominated by the Be^{2+} on account of its higher charge [29]. Considering the effect of Li^+ ion, two calculated intense bands are located at 563 and 678 cm^{-1} which are assigned to the symmetric stretch vibration of Be–F and Li–F bonds, respectively. The calculated of Raman spectrum of the Li_2BeF_4 molecule do not match well with the experimental data. This may be caused by the marginal electronic stability of Li_2BeF_4 [30]. As a result, the polymolecular structure of $4Li_2BeF_4$ was taken into account. The observed intense Raman band at 551 cm^{-1} is better reproduced by the computed frequency of $4Li_2BeF_4$ with the theoretical intense band at 579 cm^{-1}. The isolated BeF_4^{2-} anion is strongly affected by lithium ion and molten salt environment, which is similar to the other small species in melts [31,32,33].

3.4. Binary beryllium fluoride anions in molten LiF

With adding BeF_2 into the molten LiF, only one obvious intense band was observed in Raman spectra and the modes in the region of 400–600 cm^{-1} are the most informative and process the highest intensity [10]. Herein, the experimental Raman spectra of molten LiF-BeF_2 mixtures with BeF_2 varying from 20 to 80 mol% were recorded, smoothed and deconvoluted by Gaussian fuction (Fig. 6). With low concentration of BeF_2 (20 mol%) in molten LiF, the Raman spectra was almost the same with molten Li_2BeF_4 except for the reduced intensity. It is suggested that the BeF_4^{2-} anion at 551 cm^{-1} is the predominant species in molten LiF-BeF_2 with the concentration of BeF_2 below 33 mol%. When the concentration of BeF_2 reached 40 mol%, the band broaden and the position blue shifted to 517 cm^{-1} which contains two bands at 551 and 507 cm^{-1}. Further increasing the concentration of BeF_2 (50 mol%), the band shifted to 451 cm^{-1} which contain two bands at 507 and 436 cm^{-1}. Moreover, the band shifted to 436 cm^{-1} when the concentration of BeF_2 exceed 60 mol% and no band shift occurred except for the strength decreasing. It indicates that the BeF_4^{2-} tetrahedral linked one with each other through a corner-sharing mechanism, and finally formed a network analogous to pure BeF_2 [29].

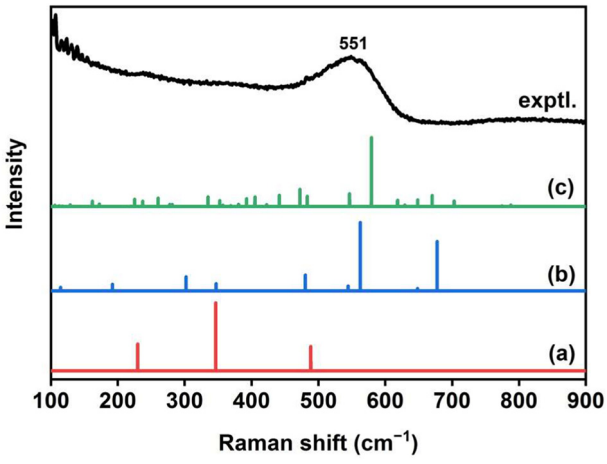

Fig. 5. Experimental Raman spectrum of molten Li_2BeF_4 (top), and calculated Raman spectra of relative structures: (a) BeF_4^{2-}, (b) Li_2BeF_4, (c) $4Li_2BeF_4$.

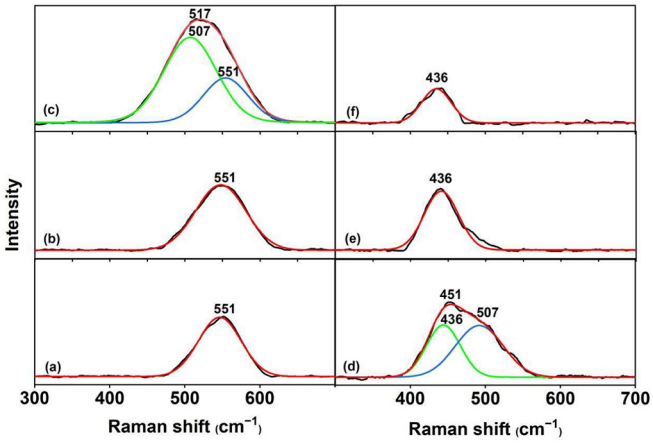

Fig. 6. The deconvolved experimental Raman spectra of the LiF-BeF_2 melts with different BeF_2 concentrations by Gaussian function: (a) 20 mol% BeF_2 at 973 K, (b) 33 mol% BeF_2 at 873 K, (c) 40 mol% BeF_2 at 873 K, (d) 50 mol% BeF_2 at 873 K, (e) 60 mol% BeF_2 at 873 K, (f) 80 mol% BeF_2 at 873 K.

3.5. Calculated Raman spectra of molten LiF-BeF_2 system

Based on the spectral features, the structure of the LiF-BeF_2 melts can be depicted as a network of BeF_4^{2-} tetrahedral ions that are connected by their corners. The Li^+ ion is also taken into account to assist the assignment of the observed bands in the experimental Raman spectrum. Three typical beryllium-fluorine tetrahedron species $Li_xBe_2F_7^{(3-x)-}$, $Li_yBe_3F_{10}^{(4-y)-}$ and $Li_zBe_6F_{18}^{(6-z)-}$ were optimized to be geometrically stable by HF/6–311+G(d) level (Fig. S4, S5 and S6 in supplementary material). According to the calculated Raman spectra (Fig. S7, S8 and S9 in supplementary material), these species are less affected by the environment and alkali metal cations [34]. As a result, the probable species were shown in Fig. 7. The structure of $LiBe_2F_7^{2-}$ anion was in the form of two BeF_4 moieties connected by one bridging fluoride with one Li^+ around. Similarly, $Be_3F_{10}^{4-}$ was connected by fluorine atoms with three BeF_4 moieties and formed a chain structure.

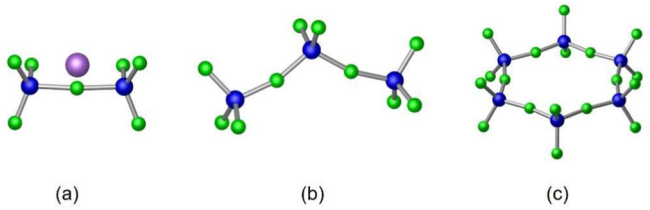

Fig. 7. Diagrams of model structure units containing different connectivities of beryllium-fluorine tetrahedral (Be: blue, F: green, Li: purple) by HF/6–311+G(d) level of theory: (a) $LiBe_2F_7^{2-}$, (b) $Be_3F_{10}^{4-}$, (c) $Be_6F_{18}^{6-}$.

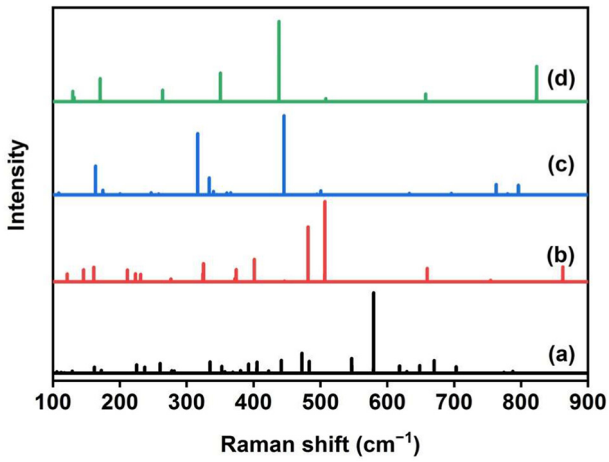

Fig. 8. Calculated Raman spectra of beryllium-fluorine tetrahedral by different connectivities by 6–311+G(d) basis set: (a) BeF_4^{2-}, (b) $Be_2F_7^{3-}$, (c) $Be_3F_{10}^{4-}$, (d) $Be_6F_{18}^{6-}$.

As to the $Be_6F_{18}^{6-}$ structure, it processed a hexatomic ring with six bridging fluoride atoms. These species are similar to the reported species of $Be_2F_7^{3-}$ and $Be_3F_{10}^{4-}$ anions [13].

The calculated Raman spectra of these different species with 6–311+G(d) basis set were presented in Fig. 8. In molten LiF-BeF_2 mixtures, only the band of symmetrical Be–F stretching vibration was obvious in the region of 400–600 cm^{-1} while other bands were not observable due to the weak Raman activities. The theoretical intense bands in this region were consistent with the experimental values (Fig. 6). The error between experimental and unscaled calculated vibrational frequencies is within 10% with a gas-phase structure for modeling the molten salt [35]. It is obvious that the observed Raman bands at 551 and 507 cm^{-1} are best fit by the results of BeF_4^{2-} and $Be_2F_7^{2-}$ with the affection of Li^+ ions. Furthermore, a well agreement can be reached if $Be_3F_{10}^{4-}$ and $Be_6F_{18}^{6-}$ are taken into account for the observed band at 436 cm^{-1}.

On the basis of the Raman spectroscopic and theoretical results, the mechanism regarding how the concentration of BeF_4 affects the speciation in molten LiF has been explained, which eventually leads to the formation of BeF_2. At high dilution in LiF (BeF_2 < 33 mol%), only BeF_4^{2-} anion was observed and predominant in the melt and affected by the marginal electronic stability. When BeF_2 concentration was increased (40 mol%), beryllium existed in the form of dimer BeF_4^{2-} and $Be_2F_7^{3-}$ following the reactions 1. Both of them were affected by the cations more or less. In addition, a second species in the form of $Be_3F_{10}^{4-}$ was produced with the concentration of BeF_2 increased to 50 mol% (Reaction 2). Further increasing the BeF_2 concentration (60 and 80 mol%), one intense band was observed in the region of 400–600 cm^{-1} and the intensity reduced severely. It indicated that the band in the spectrum approaches that of hexagonal BeF_2 in which the network structure was connected by hexatomic BeF_4 rings [36,37], and existed in the formation of $Be_6F_{18}^{6-}$ (Reaction 3).

$$2BeF_4^{2-} \leftrightarrow Be_2F_7^{3-} + F^- \quad (1)$$

$$BeF_4^{2-} + Be_2F_7^{3-} \leftrightarrow Be_3F_{10}^{4-} + F^- \quad (2)$$

$$2Be_3F_{10}^{4-} \leftrightarrow Be_6F_{18}^{6-} + 2F^- \quad (3)$$

4. Conclusions

The structural evolution of Li_2BeF_4 from the crystalline to molten state has been elucidated. Its major vibrational modes from room temperature to 823 K were assigned based on theoretical calculation. BeF_4^{2-} was formed and combined with two Li^+ at room temperature. In molten state, the BeF_4^{2-} was proved to be the predominant species which was affected by Li^+ and marginal electronic stability.

The symmetric stretching vibrational wavenumbers of beryllium-fluorine bonds in binary LiF-BeF_2 melts were determined and analyzed. Deconvolution of these bands in molten Raman spectra by using Gaussian function was carried out. An important proportion of BeF_4 tetrahedral linked one with each other through a corner-sharing mechanism, leading to the formation of a series fluoroberyllate species: BeF_4^{2-}, $Be_2F_7^{3-}$, $Be_3F_{10}^{4-}$, and $Be_6F_{18}^{6-}$. Furthermore, the experimental and theoretical results indicate that these species can be considered as intermediate during the transformation from BeF_4^{2-} to the polymer BeF_2 structure.

Declaration of Competing Interest

The authors declare that they have no known competing financial interests or personal relationships that could have appeared to influence the work reported in this paper.

Acknowledgements

This work was supported by the Strategic Priority Research Program and Frontier Science Key Program of the Chinese Academy of Sciences (Grants XDA02030000 and QYZDY-SSW-JSC016), the Young Potential Program of Shanghai Institute of Applied Physics, Chinese Academy of Sciences (E0553401).

Appendix A. Supplementary data

Supplementary data to this article can be found online at https://doi.org/10.1016/j.molliq.2020.115208.

References

[1] E. Merle-Lucotte, D. Heuer, M. Allibert, V. Ghetta, C. Le-Brun, R. Brissot, E. Liatard, L. Mathieu, The Thorium Molten Salt Reactor: Launching The Thorium Cycle While Closing The Current Fuel Cycle. European Nuclear Conference (ENC 2007), Brussels, Belgium September, 2007 48–53.
[2] Z. Dai, Thorium molten salt reactor nuclear energy system (TMSR), Molten Salt Reactors and Thorium Energy (2017) 531–540.
[3] P.N. Haubenreich, J. Engel, Experience with the molten-salt reactor experiment, Nucl. Technol. 8 (1970) 118–136.
[4] M. Rosenthal, P. Kasten, R. Briggs, Molten-salt reactors-history, status, and potential, Nucl. Technol. 8 (1970) 107–117.
[5] J. Dai, D. Long, P. Huai, Q. Li, Molecular dynamics studies of the structure of pure molten ThF_4 and ThF_4–LiF–BeF_2 melts, J. Mol. Liq. 211 (2015) 747–753.
[6] P. Seiler, Estimation of ionicity coefficients in Li_2BeF_4 crystals by X-ray diffraction, Acta Crystallogr. Sect. B: Struct. Sci. 49 (1993) 223–235.
[7] J. Burns, E. Gordon, Refinement of the crystal structure of Li_2BeF_4, Acta Crystallogr. 20 (1966) 135–138.
[8] P. Hartman, A uniform description of phenakite type structures as superstructures of β-Si_3N_4, Ztschrift für Kristallographie 187 (1989) 1–4.

[9] A.S. Quist, J.B. Bates, G.E. Boyd, Raman spectra of tetrafluoroberyllate ion in molten sodium fluoride and lithium fluoride to 686°, J. Phys. Chem. 76 (1972) 78–83.
[10] L.M. Toth, J. Bates, G.E. Boyd, Raman spectra of $Be_2F_7^{3-}$ and higher polymers of beryllium fluorides in the crystalline and molten state, J. Phys. Chem. 77 (1973) 216–221.
[11] R.J. Heaton, R. Brookes, P.A. Madden, M. Salanne, C. Simon, P. Turq, A first-principles description of liquid BeF_2 and its mixtures with LiF: 1. Potential development and pure BeF_2, J. Phys. Chem. B 110 (2006) 11454–11460.
[12] M. Salanne, C. Simon, P. Turq, R.J. Heaton, P.A. Madden, A first-principles description of liquid BeF_2 and its mixtures with LiF: 2. Network formation in LiF— BeF_2, J. Phys. Chem. B 110 (2006) 11461–11467.
[13] J. Dai, H. Han, Q. Li, P. Huai, First-principle investigation of the structure and vibrational spectra of the local structures in LiF–BeF_2 molten salts, J. Mol. Liq. 213 (2016) 17–22.
[14] S. Liu, T. Su, J. Cheng, X. An, P. Zhang, H. Liu, S. Yao, L. Xie, H. Hou, Investigation on molecular structure of molten Li_2BeF_4 (FLiBe) salt by infrared absorption spectra and density functional theory (DFT), J. Mol. Liq. 242 (2017) 1052–1057.
[15] V. Dracopoulos, B. Gilbert, G.N. Papatheodorou, Vibrational modes and structure of lanthanide fluoride-potassium fluoride binary melts LnF_3-KF (Ln = La, Ce, Nd, Sm, Dy, Yb), J. Chem. Soc., Faraday Trans 94 (1998) 2601–2604.
[16] B. Sang-Eun, J.T. Sub, C. Young-Hwan, K. Jong-Yun, K. Kyungwon, P. Tae-Hong, Electrochemical formation of divalent samarium cation and its characteristics in LiCl–KCl melt, Inorg. Chem. 57 (2018) 8299–8306.
[17] H. Peng, W. Huang, L. Xie, Q. Li, Solubility and precipitation investigations of UO_2 in LiF–BeF_2 molten salt, J. Nucl. Mater. 531 (2020) 152004.
[18] R.E. Thoma (Ed.), Phase diagrams of nuclear reactor materials, ORNL–25481959.
[19] M.D. Segall, P.J.D. Lindan, M.J. Probert, C.J. Pickard, P.J. Hasnip, S.J. Clark, M.C. Payne, First-principles simulation: ideas, illustrations and the CASTEP code, J. Phys. Condens. Matter 14 (2002) 2717.
[20] S.J. Clark, M.D. Segall, C.J. Pickard, P.J. Hasnip, M.I.J. Probert, K. Refson, M.C. Payne, First principles methods using CASTEP, Z. Kristallographie—Cryst. Mater 220 (5–6) (2005) 567–570.
[21] Z. Wu, R.E. Cohen, More accurate generalized gradient approximation for solids, Phys. Rev. B: Condens. Matter Mater. Phys. 73 (2006) 235116.
[22] M.J. Frisch, G.W. Trucks, H.B. Schlegel, G.E. Scuseria, M.A. Robb, J.R. Cheeseman, G. Scalmani, V. Barone, B. Mennucci, G.A. Petersson, et al., Gaussian 09, Revision a.01, Gaussian, Inc., Wallingford, CT, 2009.
[23] K. Raghavachari, J.S. Binkley, R. Seeger, J.A. Pople, Self-consistent molecular orbital methods. 20. Basis set for correlated wave-functions, J. Chem. Phys 72 (1980) 650–654.
[24] P. Seiler, Estimation of ionicity coefficients in Li_2BeF_4 crystals by X-ray diffraction, Acta Crystallogr. 49 (1993) 223–235.
[25] J. Burns, E.K. Gordon, Refinement of the crystal structure of Li_2BeF_4, Acta Crystallogra. 20 (1966) 135–138.
[26] V. Dracopoulos, J. Vagelatos, G. Papatheodorou, Raman spectroscopic studies of molten ZrF_4-KF mixtures and of A_2ZrF_6 A_3ZrF_7 (A = Li, K or Cs) compounds, J. Chem. Soc., Dalton Trans 7 (2001) 1117–1122.
[27] G.M. Photiadis, G.N. Papatheodorou, Vibrational modes and structure of liquid and gaseous zirconium tetrachloride and of molten $ZrCl_4$-CsCl mixtures, J. Chem. Soc. Dalton Trans. 6 (1998) 981–990.
[28] W.M. Haynes, Handbook of chemistry and physics, 96th ed CRC Press, 2015–2016.
[29] A.-L. Rollet, M. Reports, Studies of the local structures of molten metal halides, Annu. Rep. Prog. Chem., Sect. C: Phys. Chem 107 (2011) 88–123.
[30] M. Gutowski, A.I. Boldyrev, J. Simons, J. Rak, J. Błażejowski, Properties of closed-shell, octahedral, multiply-charged hexafluorometallates MF_6^{3-}, M = Sc, Y, La, ZrF_6^{2-}, and TaF_6^-, J. Am. Chem. Soc. 118 (1996) 1173–1180.
[31] H. Ohata, K. Takeuchi, K. Ui, N. Koura, The structure of molten lithium carbonate calculated by dft and md simulations, ECS Trans 6 (2007) 57–65.
[32] M. Wang, P. Simon, L. Lu, A.A. Sobol, J. You, Quantitative studies on the structure of molten binary potassium molybdates by *in situ* Raman spectroscopy and quantum chemistry *ab initio* calculations, Anal. Chem. 90 (2018) 9085–9092.
[33] V.H. Paschoal, L.F. Faria, M.C. Ribeiro, Vibrational spectroscopy of ionic liquids, Chem. Rev. 117 (2017) 7053–7112.
[34] C. Wang, X. Chen, R. Wei, Y. Gong, Raman spectroscopic and theoretical study of scandium fluoride and oxyfluoride anions in molten FLiNaK, J. Phys. Chem. B 124 (2020) 6671–6678.
[35] W.R. Carper, P.G. Wahlbeck, T.R. Griffiths, DFT models of molecular species in carbonate molten salts, J. Phys. Chem. B 116 (2012) 5559.
[36] A.F. Wright, A.N. Fitch, The preparation and structure of the α- and β-quartz polymorphs of beryllium fluoride, J. Solid State Chem. 73 (1988) 298–304.
[37] A.H. Narten, Diffraction pattern and structure of noncrystalline BeF_2 and SiO_2 at 25 °C, J. Chem. Phys. 56 (1972) 1905.